Journal of Materials Science and Chemical Engineering, 2026, 14(3), 30-45
https://www.scirp.org/journal/msce
ISSN Online: 2327-6053
ISSN Print: 2327-6045

Anisotropic Electron-Phonon Coupling in Fluorinated GeC: Ultra-Fast Hot-Carrier Thermalization from First Principles

N'goyé Bré-Junior Kanga[1,2], Boris Irie-Bi[1], Lalla Btissam Drissi[2,3,4], Abdelali Ait Taleb[2,3]

[1]Department of Physics, University of Man, Man, Côte d'Ivoire
[2]Centre of Physics and Mathematics (CPM), Faculty of Science, Mohammed V University, Rabat, Morocco
[3]LPHE, Modeling & Simulations, Faculty of Science, Mohammed V University, Rabat, Morocco
[4]College of Physical and Chemical Sciences, Hassan II Academy of Sciences and Technology, Rabat, Morocco
Email: junior.kanga@univ-man.edu.ci

How to cite this paper: Kanga, N.B.-J., Irie-Bi, B., Drissi, L.B. and Ait Taleb, A. (2026) Anisotropic Electron-Phonon Coupling in Fluorinated GeC: Ultra-Fast Hot-Carrier Thermalization from First Principles. *Journal of Materials Science and Chemical Engineering*, **14**, 30-45.
https://doi.org/10.4236/msce.2026.143004

Received: November 28, 2025
Accepted: March 9, 2026
Published: March 12, 2026

Abstract

Ultra-fast hot-carrier relaxation via electron-phonon (e-ph) coupling fundamentally limits efficiency in optoelectronic devices. This ab initio study employs density functional theory (DFT) and many-body perturbation theory to probe these dynamics in the fully fluorinated GeC (F-GeC-F) monolayer, a wide-gap 2D semiconductor with exceptional stability. Our calculations show that optical phonons dominate electron-phonon scattering, with the LO2 mode governing the VBM and the LO3 mode dominating the CBM, where scattering is significantly stronger, making LO3 the primary channel overall. This strong coupling drives ultra-fast thermalization 100 fs across 0 - 400 K, matching unfluorinated GeC despite fluorination's dramatic bandgap expansion. Pronounced anisotropy emerges in linewidths along high-symmetry k-paths, with coupling strength varying dramatically by crystallographic direction and temperature. These mode-resolved, temperature-dependent insights, nearly impossible to isolate experimentally, offer a microscopic blueprint for engineering carrier lifetimes in next-generation 2D nanoelectronics and photodetectors.

Keywords

Electron-Phonon Coupling, Fluorination, 2D Binary Monolayer, Linewidth, Relaxation Time, Thermalization, Scattering Rate

1. Introduction

The isolation of graphene in 2004 marked a turning point in materials science [1],

proving that a one-atom-thick crystal could remain stable and opening the door to an explosion of research on two-dimensional (2D) materials. Beyond graphene itself, this sparked intense exploration of related systems like silicene [2], germanene [3], phosphorene [4], stanene [5], alongside hybrid structures that stack or blend these layers to unlock tailored properties for flexible electronics, high-performance thermoelectric materials and advanced energy storage [6].

Silicene, germanene and stanene monolayers mirror graphene's semi-metallic character, with charge carriers behaving as massless Dirac fermions due to their linear $\pi - \pi^*$ band dispersion at the Fermi level [7] [8]. This gapless nature, while fascinating for fundamental studies, severely limits their utility in bandgap-dependent technologies like solar cells or light-emitting diodes. Overcoming this drawback has driven widespread efforts to engineer band gaps through strain, substrates, electric fields, quantum confinement or chemical functionalization—often yielding modest gaps that still fall short of practical requirements [9] [10].

One standout solution lies in crafting hybrid 2D alloys by intermixing group-IV elements with carbon, which breaks the lattice symmetry and reliably opens substantial bandgaps while preserving exceptional carrier mobilities. By alternating silicon, germanium, or tin atoms with carbon in a buckled hexagonal lattice, materials like SiC, GeC, and SnC emerge with direct or indirect gaps; values large enough to power real-world optoelectronics alongside the mechanical flexibility and spin-orbit effects inherited from their parent compounds [11] [12]. Recent advances have unveiled even broader potential across the family of carbon-based binary compounds. SiC monolayers stand out as highly efficient UV-absorbing materials incorporating plasmonic light trapping for next-generation photodetectors [13]. Electron-phonon dynamics studies confirm that XC (X=Si, Ge, Sn) hybrids sustain exceptionally long carrier lifetimes that are essential for high-performance transistors [14]. Non-metal adsorption on SiC/GeC further enables tunable bandgaps and induced magnetism [15]. Most strikingly, OsC emerges as a room-temperature 2D topological insulator featuring a robust bulk bandgap with metallic edge states, perfectly suited for quantum spin Hall devices [16]. Together, these properties position the family as a versatile platform spanning photonics, spintronics, and topological nanoelectronics.

The GeC hybrid monolayer merits special focus, as it can be synthesized at scale through techniques like laser ablation or radiofrequency reactive sputtering in an Ar/CH_4 atmosphere, producing freestanding films with atomic-level control [17] [18]. Recent literature has elevated g-GeC from a theoretical curiosity to a frontrunner across energy, sensing, and spintronics applications. GeC monolayer showcased its standout electrocatalytic edge as a cathode for fuel cells and Li-O_2 batteries, with overpotentials under 0.2 V for hydrogen evolution reaction (HER)/oxygen reduction reaction (ORR) and cycling stability outpacing graphene [19]. Excitonic effects and robust ~1 eV bandgaps, persisting even at 50 T fields, further unlock magneto-optoelectronics and valleytronics [20]. Doping breakthroughs amplify this versatility—non-metal adsorption (H, O, F) tunes

gaps and induces half-metallicity [15], while transition-metal substitution in g-GeC drives high-T_C ferromagnetism and magnetic anisotropy for 2D spintronics [21] [22]. Sensing prowess shines too, with GeC monolayers delivering record sensitivity and recyclability for SO_2/NO_2 detection via physical adsorption and work function shifts [23]. These advances—spanning catalysis, electronics, and quantum properties—position GeC as a uniquely tunable bridge from lab synthesis to deployable nanotech.

Building on this progress, targeted studies of GeC functionalization have explored fluorinated derivatives, examining three distinct configurations: fully fluorinated F-GeC-F and the two half-fluorinated variants F-GeC and GeC-F [24]. Each proves a stable semiconductor with impressively large bandgaps, namely 1.81 eV, 3.3 eV, and 1.77 eV respectively under GGA, jumping to 2.73 eV, 4.04 eV, and 2.22 eV with the more accurate HSE functional. These wide gaps, spanning the visible spectrum, position fluorinated GeC as a serious contender for optoelectronics where pristine hybrids fall short. Even more striking, fluorination unlocks magnetic order: F-GeC orders antiferromagnetically, while GeC-F emerges as a weak ferromagnetic semiconductor [25], all while boosting energetic stability over hydrogenation alternatives and easing lab synthesis [26] [27].

Despite these advances, a critical gap persists: while electron-phonon (e-ph) coupling has been probed in pristine or semi-fluorinated GeC, no study has delivered a mode-resolved, temperature-dependent analysis of hot-carrier relaxation in the fully fluorinated F-GeC-F monolayer; the very system poised to excel in high-performance nanoelectronics and spin-valleytronics. This absence leaves unanswered how phonon bottlenecks dictate ultrafast thermalization, carrier multiplication, and lifetime control in wide-gap 2D hybrids, directly stalling progress toward practical devices that demand precise command of non-equilibrium dynamics. Our work confronts this head-on, pioneering the first ab initio, phonon-resolved mapping of e-ph linewidths, scattering rates, and thermal susceptibility in F-GeC-F, revealing mode-specific fingerprints that unlock engineering handles for next-generation optospintronics.

Such versatility naturally draws attention to electron-phonon (e-ph) interactions, the workhorse of charge carrier dynamics in 2D materials; a field tracing back to classic explanations of metallic resistivity [28] and now central to superconductivity [29], Kohn anomalies [30], Peierls distortions [31], and polaron effects [32]. In the present work, we fill that void with a fully ab initio treatment of e-ph coupling in fluorinated GeC, leaning on density functional theory and Wannier interpolation to map the imaginary self-energy and scattering rates across phonon modes far beyond empirical approximations [33]. We also track mode-specific temperature dependence, tackling the notorious *k*-point convergence demands head-on to reveal how coupling strength varies across the Brillouin zone. At the conduction band minimum, out-of-plane transverse phonons dominate; at the valence band maximum, in-plane longitudinal and transverse modes take over. Strikingly, these peak contributors to linewidths prove the most tempera-

ture-sensitive, their stability crumbling as heat rises, while the Γ-point linewidth stays near-zero thanks to the material's gapped Fermi surface.

These patterns emerge from exhaustive phonon-resolved linewidths at band edges along high-symmetry paths, capturing all twelve branches' characteristic dispersions and their hot-electron scattering rates. The nonuniform coupling—strongest at edges, weakest at zone center—hints at tailored strategies for managing carrier lifetimes in devices.

This paper unfolds as follows. Section 2 lays out our computational approach. We then present the linewidth landscape as a function of energy and temperature, followed by mode-by-mode dissections of scattering and self-energy along key *k*-paths. Temperature effects on phonon contributions close out the results, before a final synthesis of implications.

2. Computational Methods

Our computational methodology relies on Density-Functional Theory (DFT) [34], with lattice dynamics determined via density-functional perturbation theory (DFPT) [35]. All calculations were performed using the Quantum Espresso (QE) simulation package [36] to self-consistently solve the Kohn-Sham (KS) equations [37].

For the exchange and correlation interaction, we utilized the Generalized Gradient Approximation (GGA) of Perdew, Burke, and Ernzerhof (PBE) [38], as the Local Density Approximation (LDA) is known to underestimate interatomic distances. The electronic wavefunctions were described using norm-conserving pseudopotentials [39] with a plane-wave expansion cutoff energy of 45 Ry. To simulate an isolated sheet and prevent interactions between layers, a vacuum space greater than 18 Å was implemented along the *z*-direction.

The electronic states were computed using a 32 × 32 × 1 Monkhorst-Pack *k*-sampling grid in the Brillouin Zone. The vibrational properties, specifically the frequencies $\omega_{p\lambda}$ and the derivatives of the self-consistent KS potential, were calculated on a corresponding 16 × 16 × 1 q-point grid. The e-ph coupling and the imaginary part of the e-ph self-energy $\Gamma_{n,k}$ were subsequently computed using the EPW program [40]. The fundamental quantity in this calculation is the e-ph matrix element, $g_{n,m,k}^{\lambda,q}$ defined as [41]:

$$g_{n,m,k}^{\lambda,q} = \left\langle \psi_{m,k+q} \left| \partial_{\lambda,q} V \right| \psi_{n,k} \right\rangle, \tag{1}$$

where $\psi_{n,k}$ and $\psi_{m,k+q}$ are the KS wave functions for the initial n and final m electron band indices, and $\partial_{\lambda,q} V$ is the variation of the KS potential corresponding to a phonon mode with polarization λ and wave vector q.

This matrix element is used to calculate the imaginary part of the self-energy $\Gamma_{n,k}$ via the expression [41]:

$$\Gamma_{n,k} = \sum_{m,k,q} \left| g_{n,m,k}^{\lambda,q} \right|^2 \mathrm{Im}\left[\frac{N_{\lambda,q} + 1 - f_{m,k}}{\varepsilon_{n,k} - \varepsilon_{m,k+q} - \hbar\omega_{\lambda,q} - i\eta} + \frac{N_{\lambda,q} - f_{m,k}}{\varepsilon_{n,k} - \varepsilon_{m,k+q} + \hbar\omega_{\lambda,q} - i\eta} \right] \tag{2}$$

where $\hbar\omega_{\lambda,q}$ is the phonon energy, $f_{m,k}$ and $N_{\lambda,q}$ are the Fermi and Bose oc-

cupation numbers, respectively, and η serves as a Lorentzian broadening parameter. To accurately deduce $\Gamma_{n,k}$ within EPW, the matrix elements were evaluated on a dense 160 × 160 × 1 q-point grid. Finally, the e-ph relaxation time, which is inversely proportional to the scattering rate, is computed from the self-energy as:

$$\tau_{n,k}^{e-ph} = \frac{2\Gamma_{n,k}}{\hbar} \tag{3}$$

By utilizing dense momentum grids and accurate Wannier interpolation, the study captures the overriding influence of acoustic and optical phonon modes. Although germanium is a relatively heavy element, spin-orbit coupling (SOC) was omitted from the electronic structure calculations.

All computational methods reported here were performed for the two possible configurations of the half-fluorinated GeC hybrid.

3. Results and Discussion

3.1. Electron Linewidth versus Temperature

The chemical functionalization of the planar GeC sheet by fluorine disrupts its native π-bonding network, inducing a re-hybridization of the carbon and germanium atoms to an sp^3 state. Consequently, the planar structure of GeC transforms into a puckered conformation. The calculations in this work focus on this fully fluorinated system, specifically in its stable chair conformer. As depicted in Figure 1, this structure features fluorine atoms bonded to carbon on one side of the sheet and to germanium on the opposite side, creating an alternating "1-up/1-down" arrangement.

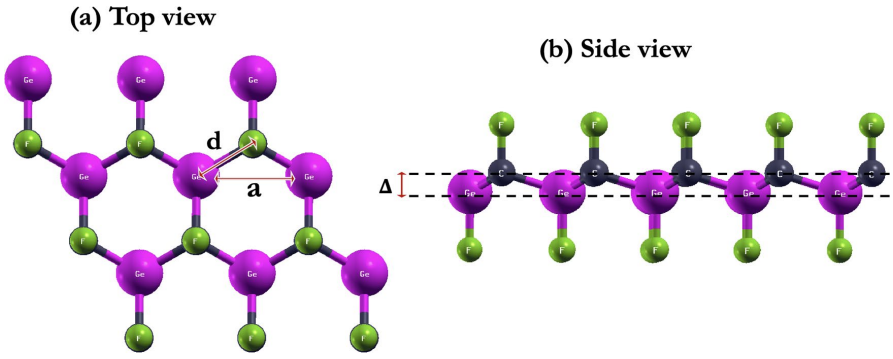

Figure 1. Fully fluorinated GeC atomic structure: (a) Top view and (b) slide view. The lattice parameter a = 3.33 Å, the bond length Ge-C d = 2.02 Å, the buckling Δ = 0.60 Å.

In the following, we apply this formalism to investigate the effect of full fluorination on the e-ph interaction in the GeC sheet. We conduct a detailed analysis of how different phonon modes contribute to the electron linewidth, tracking these contributions as a function of temperature and electronic energy along the high-symmetry lines of the Brillouin zone. The results of this investigation are presented in Figure 2, which displays the electronic band structure overlaid with

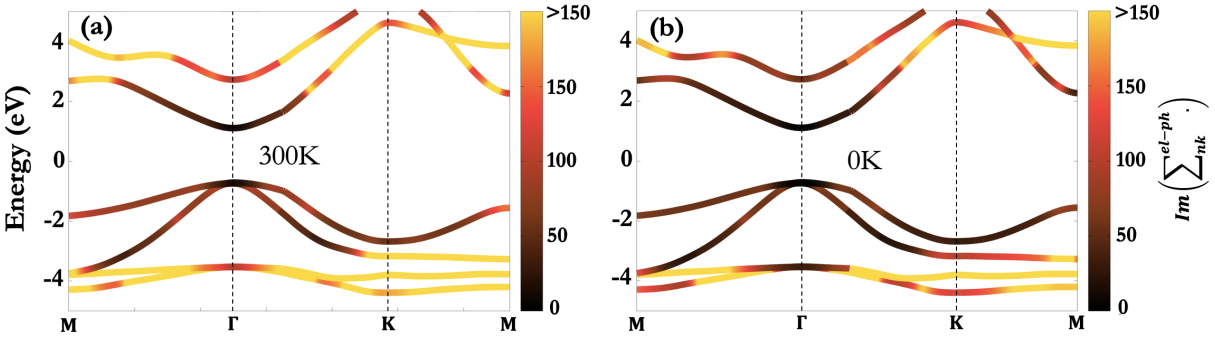

Figure 2. Imaginary part of the electron self-energy $\Gamma_{n,k}$ due to electron-phonon coupling on top of the band structure of the fully fluorinated GeC at (a) 300 K and (b) 0 K.

the imaginary part of the self-energy, calculated on a fine *k*-grid for both 0 K and 300 K. It is worth noting that understanding the thermalization of hot carriers depends on analyzing the rate of e-ph processes. This rate is quantitatively described by the imaginary part of the electron self-energy $\Gamma_{n,k}$ expressed in Equation (2). The evaluation of this electron linewidth, as detailed in [41], requires a simultaneous consideration of the e-ph matrix elements, energy conservation, and phase space occupation.

As shown in **Figure 2(b)**, a non-negligible electron linewidth emerges for states located away from the band gap, specifically impacting electrons in the higher conduction bands and holes in the lower valence bands. Consistent with the 0K condition, where thermal excitations are frozen and phonon absorption is suppressed, this observed e-ph interaction originates purely from spontaneous phonon emission. This entire analysis, which links specific scattering rates to carrier energy levels, is enabled by plotting the linewidth as a function of energy along the high-symmetry path.

As expected, the linewidth is negligible at the Γ-point for both the VBM and the CBM. This minimal scattering is a direct result of the limited phase space available for transitions, specifically the very low density of electronic states at the band edges. A small δ-function width of 0.005 eV was employed in the calculations to accurately resolve these small linewidth values.

At 300 K, **Figure 2(a)**, the linewidth becomes significantly enhanced, particularly near the Γ-K path, reflecting the thermal activation of phonon absorption channels. Regions with relatively flat dispersion, such as the deep valence bands below −4 eV, exhibit higher linewidths due to the larger density of electronic states and reduced carrier velocity. In contrast, states around the band gap show negligible linewidth, consistent with the absence of available electronic states for scattering. These observations confirm the strong temperature dependence of the electron-phonon coupling in fully fluorinated GeC and highlight the dominant role of thermally activated phonon modes in carrier relaxation at room temperature.

The choice to investigate hot carrier behavior in fully fluorinated GeC at 300 K, rather than at another temperature, is motivated by our aim to study this behavior

under room-temperature conditions.

Plotting the electron linewidth over the band structure provides a direct visualization of how electron-phonon interactions vary across different electronic states. It highlights regions where electrons experience stronger scattering and shorter lifetimes. This approach gives valuable insight into the strength and distribution of electron-phonon coupling within the material.

3.2. Scattering Rate and Lifetime

In this present work, the electron-electron interaction is neglected, as the e-ph contribution is the dominant scattering mechanism near the Fermi level. This assumption is justified for fully fluorinated GeC, where the very low electron density and the small energy range around the band edge ensure that electrons interact primarily with phonons. This approach is well-supported by previous studies [42] [43], including key work on hot carriers in silicon.

The total e-ph scattering rate, which arises from the combined contributions of both acoustic and optical phonons, is therefore the focus of our analysis. A critical factor influencing this rate is temperature. An increase in temperature enhances lattice vibrations, which in turn expands the available phase space for scattering events.

Consequently, this process amplifies the scattering rates in both the valence and conduction bands. This trend is clearly quantified in **Figure 3(a)**, which plots the scattering rate versus electron energy. A direct comparison of the 0 K and 300 K data **Figure 3(a)** vividly illustrates this temperature-induced increase, providing a precise quantification of the electron linewidth's dependence on temperature. This temperature-driven increase in scattering is also directly reflected in the linewidths presented in **Figure 2**, as the linewidth itself is a quantitative measure of the total scattering rate.

The hot carrier relaxation time $\tau_{n,k}^{e-ph}$, which is inversely proportional to the imaginary part of the self-energy, is fundamentally dictated by the available phase space for scattering. Consequently, electronic energy windows populated with a higher density of bands facilitate a larger number of possible transitions, resulting in a faster (shorter) e-ph relaxation time. This general behavior is consistent with previous findings for pristine and semi-fluorinated GeC [14] [44].

This principle is clearly illustrated by our results, as depicted in **Figure 3(b)**. Near the band edges, where the density of states is limited, $\tau_{n,k}^{e-ph}$ exhibits a correspondingly high value, indicating slower relaxation. Our analysis quantifies the hot electron lifetime at 50 - 100 fs near the Fermi level at room temperature. Conversely, for hot carriers with excess energy 200 meV or more from the Fermi level, the relaxation time shortens dramatically to less than 20 fs as more transition pathways become accessible.

Interestingly, this 50 - 100 fs lifetime is nearly identical to the ≈100 fs relaxation time recently reported for unfluorinated GeC [14]. This suggests that full fluorination does not significantly alter the hot carrier dynamics, an observation we

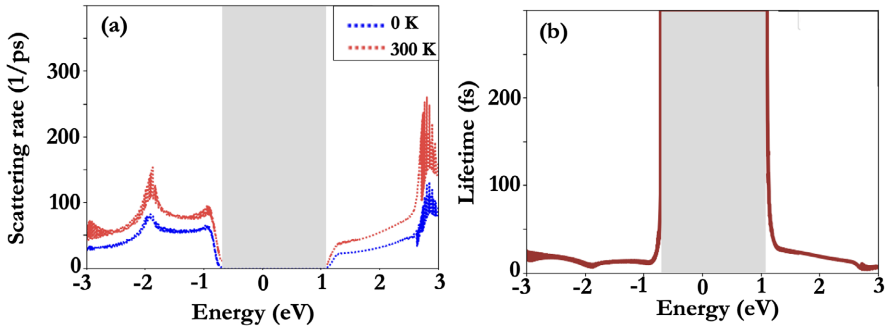

Figure 3. Electron scattering rate at 0 K and 300 K and corresponding lifetime.

attribute to the conservation of the material's direct band gap nature. This contrasts sharply with semi-fluorinated GeC with F bonded to C, which was found to have much slower relaxation [44]. That system's indirect band gap inherently restricts the efficient e-ph scattering pathways that are available in its direct-gap for pristine and fully-fluorinated counterparts.

This investigation into carrier relaxation is therefore critical for assessing the material's practical applications. Since the calculated linewidth is inversely related to the relaxation time, it provides a direct probe of the hot-carrier dynamics. Such information is fundamentally essential for the engineering of hot-carrier devices, where the primary objective is to extract carriers before they lose their excess energy through thermalization.

To identify the specific e-ph scattering pathways responsible for this rapid relaxation, we performed a quantitative analysis of the contributions from individual phonon modes to the scattering rates, as shown in **Figure 4** for 0 K and 300 K. The analysis reveals a clear distinction between the contributions of acoustic and optical modes.

For the acoustic modes, the out-of-plane acoustic (ZA) modes provide a substantial contribution in the conduction band at both temperatures 0 K and 300 K, dominating the other acoustic modes. In contrast, the situation in the valence band is temperature-dependent: the longitudinal acoustic LA mode contribution is dominant at 0 K, whereas the ZA mode becomes dominant at room temperature 300 K. This strong contribution from the temperature-sensitive ZA mode is consistent with observations made for other 2D materials like silicene and germanene [45].

Regarding the optical modes, their contributions appear less sensitive to temperature variations. In the conduction band, the LO2, LO3, and TO2 modes are the main contributors at both temperatures. Similarly, in the valence band near the band edge, the longitudinal optical LO2 mode provides the dominant contribution and is also not significantly affected by temperature.

Based on these results, we can deduce that optical modes have a higher overall contribution to the scattering rates compared to acoustic modes. The ability to compute these detailed scattering rates in the absence of experimental data highlights the benefit of the present approach for predicting material properties.

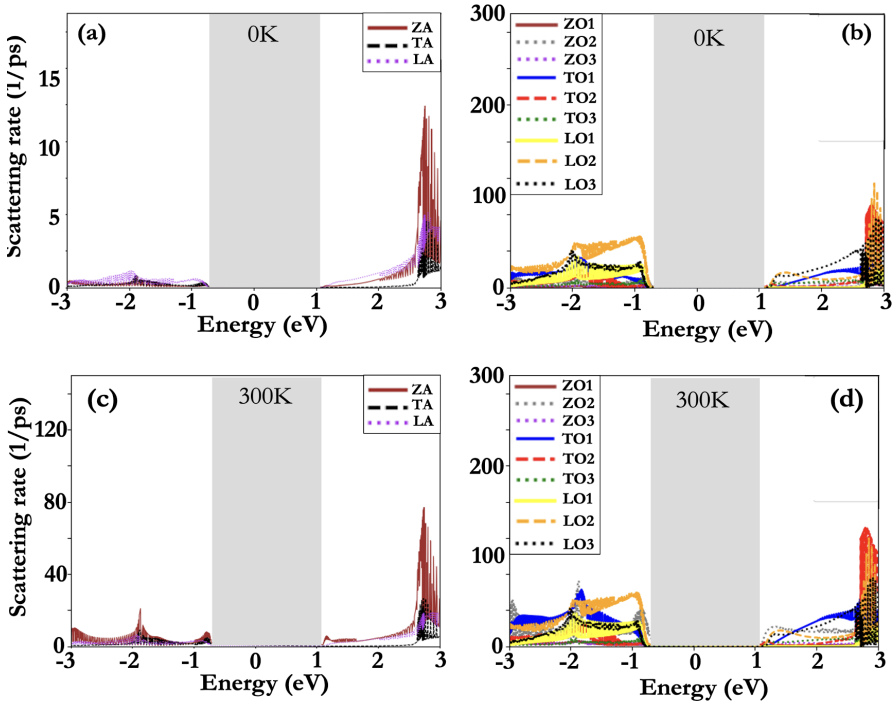

Figure 4. Temperature-dependent contribution of individual phonon modes (acoustic and optical) to the e-ph scattering rate at 0 K and 300 K.

3.3. *k*-Dependence of the Linewidth

Beyond the total scattering rates at the band extrema, a more detailed understanding requires examining the momentum k-dependence of these interactions. To this end, Figure 5 and Figure 6 display the e-ph coupling linewidth projected onto longitudinal and transversal phonon modes along the high symmetry lines of the Brillouin Zone at 0 K and 300 K.

At the VBM, as shown in Figure 5, the contributions from acoustic and optical modes are distinct. For acoustic phonons, the linewidth at 0 K is mainly due to the LA mode across the entire BZ (Figure 5(a)). At 300 K, however, the configuration changes significantly, and the major contribution shifts to the ZA mode (Figure 5(c)), confirming its high sensitivity to temperature. In contrast, the optical phonons (Figure 5(b), Figure 5(d)) exhibit much larger linewidths, dominating the acoustic contributions over the whole BZ except at Γ point. At 0 K, the coupling is dominated by the LO2 mode, which represents the primary phonon emission process responsible for thermalization process. At 300 K, the contribution from the TO1 mode increases substantially due to the larger phonon population, becoming the dominant coupling partner. Thus, the overall temperature sensitivity at the VBM arises from both the TO1 optical mode and the ZA acoustic mode.

At the CBM, detailed in Figure 6, a different set of mechanisms is dominant. Among the acoustic modes, the ZA mode provides the strongest coupling and is, again, highly sensitive to temperature. However, the primary interaction is with the optical modes. At 0 K, the phonon emission process is clearly dominated by

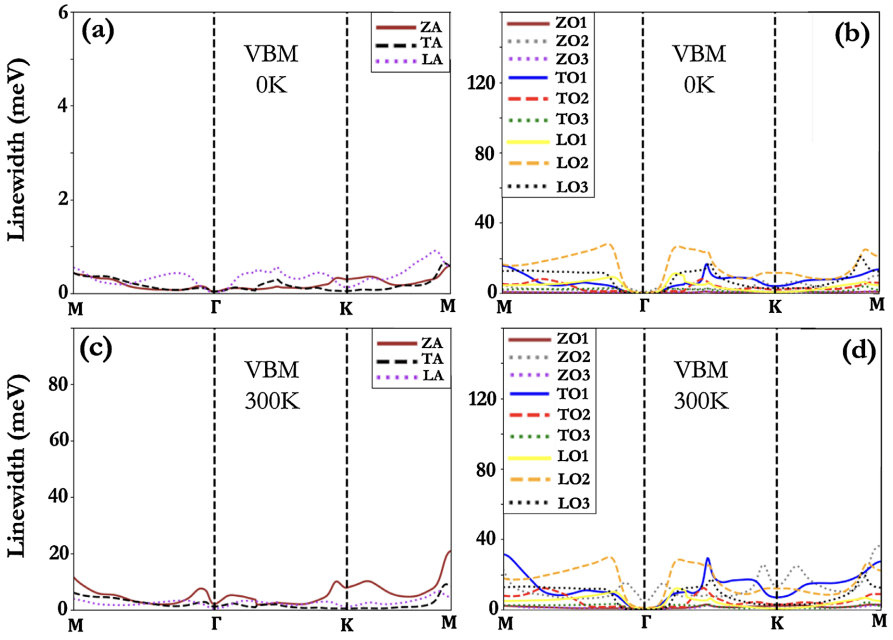

Figure 5. Momentum-resolved electron-phonon coupling linewidth at the VBM along the high symmetry lines of the Brillouin Zone. Panels (a) and (b) show the contributions from acoustic and optical phonon modes at 0 K, respectively, while panels (c) and (d) present the corresponding contributions at 300 K.

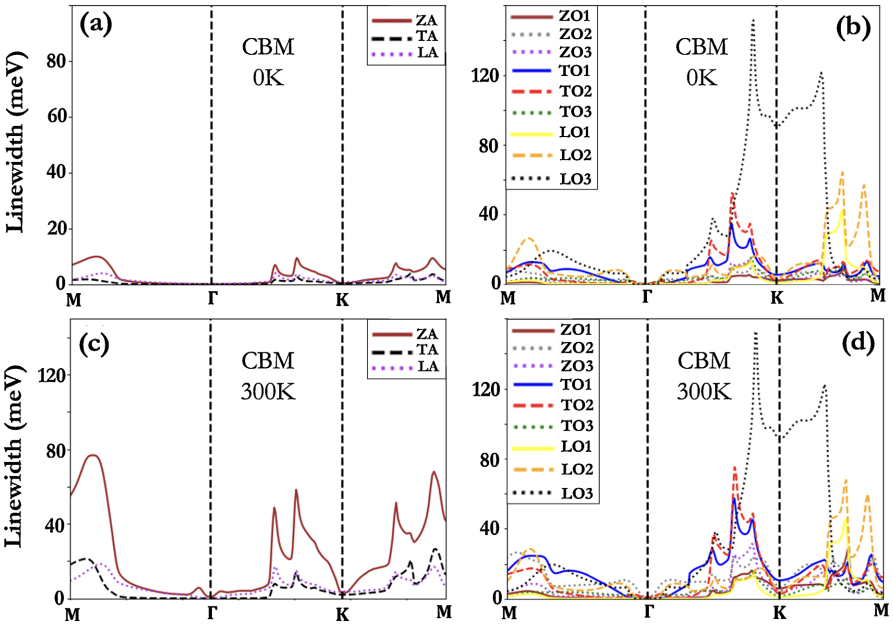

Figure 6. Momentum-resolved electron-phonon coupling linewidth at the CBM along the high symmetry lines of the Brillouin Zone. Panels (a) and (b) show the contributions from acoustic and optical phonon modes at 0 K, respectively, while panels (c) and (d) present the corresponding contributions at 300 K.

the longitudinal optical LO3 mode, particularly around the K point. This LO3 mode remains the most dominant contributor at 300K and, notably, is not very sensitive to temperature. Based on these findings, we conclude that the main ther-

malization process at the CBM is governed by the LO3 optical mode, while the overall temperature sensitivity of the coupling is driven by the ZA acoustic mode.

3.4. Mode-Resolved Thermal Analysis

At the VBM, as can be seen in Figure 7(a), the acoustic mode contributions are characterized by the out-of-plane acoustic ZA mode. The linewidth of the ZA mode exhibits a near-linear dependence on temperature, establishing it as the dominant acoustic contributor at elevated temperatures. In contrast, the contributions from the transverse TA and longitudinal LA acoustic modes are significantly smaller and display only a weaker temperature dependence. For the optical branches at the VBM, Figure 7(b) shows that, their overall linewidths are substantially larger than their acoustic counterparts. At temperatures below 150 K, the linewidth is primarily governed by the LO2 mode, followed by LO3. As temperature increases from 150 K to 400 K, the TO1 and ZO2 modes demonstrate greater temperature sensitivity, and the coupling hierarchy shifts. In this higher temperature regime, the dominant contributions come from LO2, followed by TO1 and ZO2. Nevertheless, the LO2 mode remains the principal optical contributor across the entire 0 - 400 K range, which is consistent with the findings in Figure 5.

Turning to the CBM, as depicted in Figure 7(c) shows that the ZA mode is again the most dominant acoustic contribution, with a linewidth that grows sharply with temperature, while the TA and LA modes remain subdominant. The optical mode behavior at the CBM (Figure 7(d)) is distinct. Here, the longitudinal LO3 mode provides the highest contribution to the linewidth by a significant

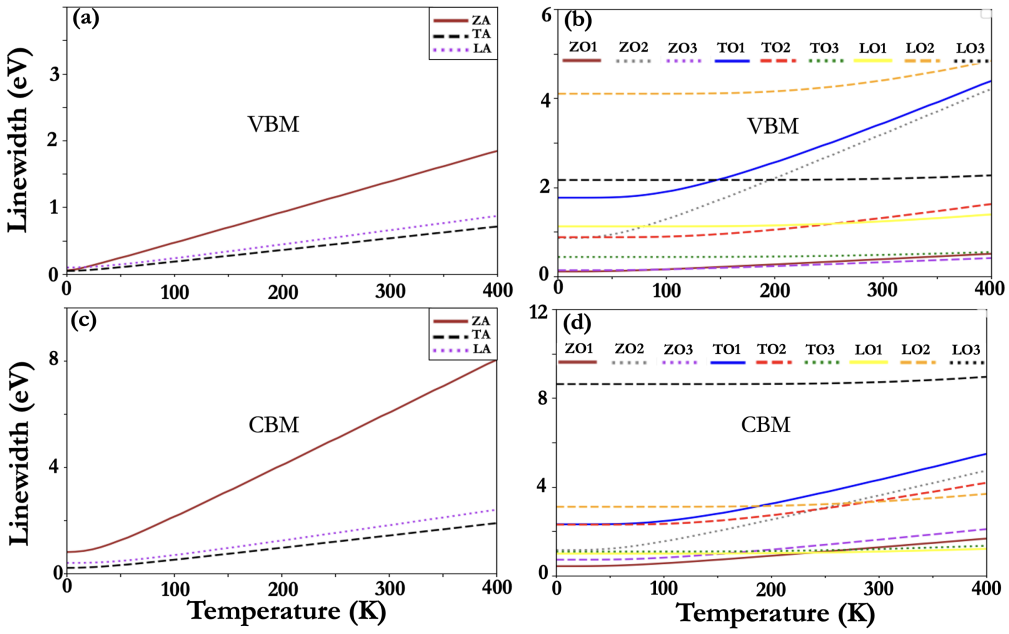

Figure 7. Mode-resolved e-ph coupling linewidth as a function of temperature at the electronic band edge. (a), (b) Acoustic and Optical mode contributions at the VBM, respectively. (c), (d) Acoustic and Optical mode contributions at the CBM, respectively.

margin. However, this dominant LO3 mode, along with the LO2 mode, displays the lowest sensitivity to temperature variations compared to the other optical branches.

A direct comparison reveals notable differences between the band edges. The absolute acoustic linewidth at the CBM is appreciably larger than at the VBM. Moreover, the ZA mode at the CBM is more temperature-sensitive than its VBM counterpart. The primary source of optical coupling also differs significantly. Indeed, while the LO2 mode governs the VBM, the LO3 mode overwhelmingly dominates at the CBM.

4. Conclusions

This comprehensive investigation delivers the first mode-resolved, temperature-dependent mapping of electron-phonon coupling in the fully fluorinated GeC monolayer (F-GeC-F), illuminating the microscopic origins of hot-carrier dynamics in this promising wide-gap 2D semiconductor. Our key findings reshape understanding of carrier relaxation in fluorinated hybrids. Optical phonons reign supreme, with the longitudinal LO3 mode identified as the overwhelming driver of e-ph scattering across the Brillouin zone. More specifically, the LO3 mode dominates scattering near the conduction band minimum (CBM), whereas the longitudinal in-plane optical mode LO2 dominates near the valence band maximum (VBM). This mode-specific fingerprint explains the ultra-fast thermalization timescale of approximately 100 fs, persisting from 0 - 400 K and remarkably matching pristine GeC despite fluorination's transformative effects on electronic structure.

Pronounced anisotropy emerges as a defining signature: linewidth magnitudes vary dramatically along high-symmetry paths, reflecting strong k-dependent coupling that scales nonlinearly with electron energy and temperature. The most influential scattering modes prove thermally fragile, their contributions surging with heat, while **Γ**-point linewidths remain suppressed due to the material's wide bandgap.

These insights carry profound implications for device engineering. The orientation-dependent transport suggests nanostructure alignment along low-coupling axes could extend carrier lifetimes for hot-carrier solar cells, while rapid relaxation favors high-speed transistors and photodetectors. Fluorinated GeC thus emerges as a tunable platform where crystallographic design, doping, and strain can dial in optimal non-equilibrium dynamics. By conquering the notorious k-point convergence challenges through Wannier interpolation and exhaustive phonon-resolved calculations, this work provides experimentalists with an atomic-level blueprint—data uniquely accessible through ab initio methods—for harnessing 2D hybrid semiconductors in next-generation nanoelectronics.

Acknowledgements

N. B.-J. Kanga and B. Irie-Bi gratefully acknowledge the Université Polytechnique

de Man (Côte d'Ivoire) for providing technical support and access to computing facilities used for the calculations. The authors thank the Laboratory of Physics of High Energies—Modelisation and Simulation (LPHE-MS), Faculty of Sciences, Mohammed V University in Rabat, Morocco, for valuable collaboration and support.

Data Availability Statement

The data that support the findings of this study are available upon reasonable request from the authors.

Conflicts of Interest

The authors declare that they have no known competing financial interests or personal relationships that could have appeared to influence the work reported in this paper.

References

[1] Novoselov, K.S., Geim, A.K., Morozov, S.V., Jiang, D., Zhang, Y., Dubonos, S.V., *et al.* (2004) Electric Field Effect in Atomically Thin Carbon Films. *Science*, **306**, 666-669. https://doi.org/10.1126/science.1102896

[2] Aufray, B., Kara, A., Vizzini, S., Oughaddou, H., Léandri, C., Ealet, B., *et al.* (2010) Graphene-Like Silicon Nanoribbons on Ag(110): A Possible Formation of Silicene. *Applied Physics Letters*, **96**, Article 183102. https://doi.org/10.1063/1.3419932

[3] Bianco, E., Butler, S., Jiang, S., Restrepo, O.D., Windl, W. and Goldberger, J.E. (2013) Stability and Exfoliation of Germanane: A Germanium Graphane Analogue. *ACS Nano*, **7**, 4414-4421. https://doi.org/10.1021/nn4009406

[4] Drissi, L.B., Sadki, S. and Sadki, K. (2018) Phosphorene under Strain: Electronic, Mechanical and Piezoelectric Responses. *Journal of Physics and Chemistry of Solids*, **112**, 137-142. https://doi.org/10.1016/j.jpcs.2017.09.017

[5] Zhu, F., Chen, W., Xu, Y., Gao, C., Guan, D., Liu, C., *et al.* (2015) Epitaxial Growth of Two-Dimensional Stanene. *Nature Materials*, **14**, 1020-1025. https://doi.org/10.1038/nmat4384

[6] Ding, T., Jiang, X., Quan, J., Wang, R., Li, M., Lan, C., *et al.* (2025) Recent Progress in Two-Dimensional Van Der Waals Heterojunctions for Flexible Energy Storage Applications. *Advanced Composites and Hybrid Materials*, **8**, Article No. 324. https://doi.org/10.1007/s42114-025-01410-1

[7] Ni, Z., Liu, Q., Tang, K., Zheng, J., Zhou, J., Qin, R., *et al.* (2012) Tunable Bandgap in Silicene and Germanene. *Nano Letters*, **12**, 113-118. https://doi.org/10.1021/nl203065e

[8] Kanga, N.B.J., Insad, S. and Drissi, L.B. (2018) Electron-Phonon Investigation in Stanene. *Computational Materials Science*, **155**, 63-68. https://doi.org/10.1016/j.commatsci.2018.08.038

[9] Gao, N., Li, J.C. and Jiang, Q. (2014) Bandgap Opening in Silicene: Effect of Substrates. *Chemical Physics Letters*, **592**, 222-226. https://doi.org/10.1016/j.cplett.2013.12.036

[10] Ouarrad, H., Drissi, L.B., Assad, R. and Fritzsche, W. (2024) Photoluminescence Mechanism and Optoelectronic Responses of Janus Pyrene and Janus Coronene QDs

for OLEDs & Nanomedical Applications. *Journal of Physics and Chemistry of Solids*, **184**, Article 111675. https://doi.org/10.1016/j.jpcs.2023.111675

[11] Drissi, L.B., Saidi, E.H., Bousmina, M. and Fassi-Fehri, O. (2012) DFT Investigations of the Hydrogenation Effect on Silicene/Graphene Hybrids. *Journal of Physics*: *Condensed Matter*, **24**, Article 485502. https://doi.org/10.1088/0953-8984/24/48/485502

[12] Zhang, J., Ren, J., Fu, H., Ding, Z., Li, H. and Meng, S. (2015) Two-Dimensional Silicon-Carbon Hybrids with a Honeycomb Lattice: New Family for Two-Dimensional Photovoltaic Materials. *Science China Physics*, *Mechanics & Astronomy*, **58**, Article 106801. https://doi.org/10.1007/s11433-015-5703-6

[13] Drissi, L.B., Ramadan, F.Z., Ferhati, H., Djeffal, F. and Kanga, N.B. (2019) New Highly Efficient 2D SiC UV-Absorbing Material with Plasmonic Light Trapping. *Journal of Physics: Condensed Matter*, **32**, Article 025701. https://doi.org/10.1088/1361-648x/ab3ab6

[14] Drissi, L.B., Kanga, N.B., Lounis, S., Djeffal, F. and Haddad, S. (2019) Electron-Phonon Dynamics in 2D Carbon Based-Hybrids XC (X=Si, Ge, Sn). *Journal of Physics: Condensed Matter*, **31**, Article 135702. https://doi.org/10.1088/1361-648x/aaff3b

[15] Ha, C.V., Ha, L.T., Hue, D.T., Nguyen, D.K., Anh, D.T., Guerrero-Sanchez, J., *et al.* (2023) First-Principles Study of SiC and GeC Monolayers with Adsorbed Non-Metal Atoms. *RSC Advances*, **13**, 14879-14886. https://doi.org/10.1039/d3ra01372c

[16] Bentaibi, B., Drissi, L.B., Saidi, E.H. and Bousmina, M. (2022) New Room-Temperature 2D Hexagonal Topological Insulator OsC: First Principle Calculations. *Materials Science in Semiconductor Processing*, **151**, Article 107009. https://doi.org/10.1016/j.mssp.2022.107009

[17] Shafi, H.Z., Mahmood, A., Ali, Z. and Mehmood, M. (2010) Optical and Structural Analysis of GeC Thin Films Deposited by Reactive Pulsed Laser Ablation Technique. *Key Engineering Materials*, **442**, 178-186. https://doi.org/10.4028/www.scientific.net/kem.442.178

[18] Hu, C.Q., Zheng, W.T., Zheng, B., Li, J.J., *et al.* (2004) Chemical Bonding of A-Ge1-xCx: H Films Grown by RF Reactive Sputtering. *Vacuum*, **77**, 63-68. https://doi.org/10.1016/j.vacuum.2004.08.004

[19] Ji, Y., Dong, H., Hou, T. and Li, Y. (2018) Monolayer Graphitic Germanium Carbide (g-GeC): The Promising Cathode Catalyst for Fuel Cell and Lithium-Oxygen Battery Applications. *Journal of Materials Chemistry A*, **6**, 2212-2218. https://doi.org/10.1039/c7ta10118j

[20] Drissi, L.B. and Ramadan, F.Z. (2015) Excitonic Effects in GeC Hybrid: Many-Body Green's Function Calculations. *Physica E*: *Low-dimensional Systems and Nanostructures*, **74**, 377-381. https://doi.org/10.1016/j.physe.2015.07.030

[21] Fan, X., Jiang, J., Li, R. and Mi, W. (2021) Half-Metallicity and Magnetic Anisotropy in Transition-Metal-Atom-Doped Graphitic Germanium Carbide (g-GeC) Monolayers. *The Journal of Physical Chemistry C*, **125**, 13688-13695. https://doi.org/10.1021/acs.jpcc.1c04139

[22] Taleb, A.A., Drissi, L.B., Kanga, N.B.J. and Lounis, S. (2024) Half-Metallic Ferromagnetism with High Critical Temperatures in Substitutionally Doped Rare-Earth 2D Germanene. *Journal of Magnetism and Magnetic Materials*, **606**, Article 172392. https://doi.org/10.1016/j.jmmm.2024.172392

[23] Li, J., Li, Z., Li, J., Hu, Z., Kang, M., Xiong, T., *et al.* (2024) GeC Monolayer: A Promising 2D Material for Reusable SO_2 and NO_2 Gas Sensor with High Sensitivity. *Materials Today Communications*, **40**, Article 110085. https://doi.org/10.1016/j.mtcomm.2024.110085

[24] Drissi, L.B., Kanga, N.B.J. and Ramadan, F.Z. (2018) Excitonic and Fluorination Effects on Optoelectronic Response of GeC Hybrid. *Computational Condensed Matter*, **14**, 49-54. https://doi.org/10.1016/j.cocom.2017.12.003

[25] Drissi, L.B., Ramadan, F.Z. and Kanga, N.B.J. (2016) Fluorination-Control of Electronic and Magnetic Properties in GeC-Hybrid. *Chemical Physics Letters*, **659**, 148-153. https://doi.org/10.1016/j.cplett.2016.07.017

[26] Karlický, F., Kumara Ramanatha Datta, K., Otyepka, M. and Zbořil, R. (2013) Halogenated Graphenes: Rapidly Growing Family of Graphene Derivatives. *ACS Nano*, **7**, 6434-6464. https://doi.org/10.1021/nn4024027

[27] Vu, T.V., Anh, N.T.T., Tran, D.P., Hoat, D.M., Binh, N.T.T., Tong, H.D., *et al.* (2020) Surface Functionalization of GeC Monolayer with F and Cl: Electronic and Optical Properties. *Superlattices and Microstructures*, **137**, Article 106359. https://doi.org/10.1016/j.spmi.2019.106359

[28] Giustino, F. (2017) Electron-Phonon Interactions from First Principles. *Reviews of Modern Physics*, **89**, Article 015003. https://doi.org/10.1103/revmodphys.89.015003

[29] Bardeen, J., Cooper, L.N. and Schrieffer, J.R. (1957) Theory of Superconductivity. *Physical Review*, **108**, 1175-1204. https://doi.org/10.1103/physrev.108.1175

[30] Kohn, W. (1959) Image of the Fermi Surface in the Vibration Spectrum of a Metal. *Physical Review Letters*, **2**, 393-394. https://doi.org/10.1103/physrevlett.2.393

[31] Peierls, R.E. (1955) Quantum Theory of Solids. Oxford University Press.

[32] Coropceanu, V., Cornil, J., da Silva Filho, D.A., Olivier, Y., Silbey, R. and Brédas, J. (2007) Charge Transport in Organic Semiconductors. *Chemical Reviews*, **107**, 926-952. https://doi.org/10.1021/cr050140x

[33] Giustino, F., Cohen, M.L. and Louie, S.G. (2007) Electron-Phonon Interaction Using Wannier Functions. *Physical Review B*, **76**, Article 165108. https://doi.org/10.1103/physrevb.76.165108

[34] Hohenberg, P. and Kohn, W. (1964) Inhomogeneous Electron Gas. *Physical Review*, **136**, B864-B871. https://doi.org/10.1103/physrev.136.b864

[35] Baroni, S., Giannozzi, P. and Testa, A. (1987) Green's-Function Approach to Linear Response in Solids. *Physical Review Letters*, **58**, 1861-1864. https://doi.org/10.1103/physrevlett.58.1861

[36] Giannozzi, P., Baroni, S., Bonini, N., Calandra, M., Car, R., Cavazzoni, C., *et al.* (2009) QUANTUM ESPRESSO: A Modular and Open-Source Software Project for Quantum Simulations of Materials. *Journal of Physics: Condensed Matter*, **21**, Article 395502. https://doi.org/10.1088/0953-8984/21/39/395502

[37] Kohn, W. and Sham, L.J. (1965) Self-Consistent Equations Including Exchange and Correlation Effects. *Physical Review*, **140**, A1133-A1138. https://doi.org/10.1103/physrev.140.a1133

[38] Perdew, J.P., Burke, K. and Ernzerhof, M. (1996) Generalized Gradient Approximation Made Simple. *Physical Review Letters*, **77**, 3865-3868. https://doi.org/10.1103/physrevlett.77.3865

[39] Hamann, D.R., Schlüter, M. and Chiang, C. (1979) Norm-Conserving Pseudopotentials. *Physical Review Letters*, **43**, 1494-1497. https://doi.org/10.1103/physrevlett.43.1494

[40] Noffsinger, J., Giustino, F., Malone, B.D., Park, C., Louie, S.G. and Cohen, M.L. (2010) EPW: A Program for Calculating the Electron-Phonon Coupling Using Maximally Localized Wannier Functions. *Computer Physics Communications*, **181**, 2140-2148. https://doi.org/10.1016/j.cpc.2010.08.027

[41] Tandon, N., Albrecht, J.D. and Ram-Mohan, L.R. (2015) Electron-Phonon Coupling and Associated Scattering Rates in Diamond. *Diamond and Related Materials*, **56**, 1-5. https://doi.org/10.1016/j.diamond.2015.03.019

[42] Shah, J. (2013) Phonon Dynamics, Ultrafast Spectroscopy of Semiconductors and Semiconductor Nanostructures. Springer.

[43] Bernardi, M., Vigil-Fowler, D., Lischner, J., Neaton, J.B. and Louie, S.G. (2014) Ab Initiostudy of Hot Carriers in the First Picosecond after Sunlight Absorption in Silicon. *Physical Review Letters*, **112**, Article 257402. https://doi.org/10.1103/physrevlett.112.257402

[44] Kanga, N.B.J., Taleb, A.A. and Drissi, L.B. (2024) Impact of Magnetism on (e-pH) Self-Energy and Thermalization of Hot Carriers in 2D Half-Functionalized GeC-Hybrid. *Physica E*: *Low-Dimensional Systems and Nanostructures*, **162**, Article 116005. https://doi.org/10.1016/j.physe.2024.116005

[45] Fischetti, M.V. and Vandenberghe, W.G. (2016) Mermin-Wagner Theorem, Flexural Modes, and Degraded Carrier Mobility in Two-Dimensional Crystals with Broken Horizontal Mirror Symmetry. *Physical Review B*, **93**, Article 155413. https://doi.org/10.1103/physrevb.93.155413